



PYFLOW_2.0: a computer program for calculating flow properties and impact parameters of past dilute pyroclastic density currents based on field data

Fabio Dioguardi¹ · Daniela Mele²

Received: 9 August 2017 / Accepted: 21 December 2017
© The Author(s) 2018. This article is an open access publication

Abstract

This paper presents PYFLOW_2.0, a hazard tool for the calculation of the impact parameters of dilute pyroclastic density currents (DPDCs). DPDCs represent the dilute turbulent type of gravity flows that occur during explosive volcanic eruptions; their hazard is the result of their mobility and the capability to laterally impact buildings and infrastructures and to transport variable amounts of volcanic ash along the path. Starting from data coming from the analysis of deposits formed by DPDCs, PYFLOW_2.0 calculates the flow properties (e.g., velocity, bulk density, thickness) and impact parameters (dynamic pressure, deposition time) at the location of the sampled outcrop. Given the inherent uncertainties related to sampling, laboratory analyses, and modeling assumptions, the program provides ranges of variations and probability density functions of the impact parameters rather than single specific values; from these functions, the user can interrogate the program to obtain the value of the computed impact parameter at any specified exceedance probability. In this paper, the sedimentological models implemented in PYFLOW_2.0 are presented, program functionalities are briefly introduced, and two application examples are discussed so as to show the capabilities of the software in quantifying the impact of the analyzed DPDCs in terms of dynamic pressure, volcanic ash concentration, and residence time in the atmosphere. The software and user's manual are made available as a downloadable electronic supplement.

Keywords Dilute pyroclastic density currents · Explosive volcanic eruptions · Hazard assessment · Dynamic pressure · Impact parameters · Deposition rate · Simulation software

Introduction

Dilute pyroclastic density currents (hereafter DPDCs) are turbulent multiphase gravity flows that can occur during explosive volcanic eruptions. While the process that generates

DPDCs can vary significantly, spanning from the collapse of an ash cloud to a direct lateral blast related to a volcanic dome collapse (Dellino et al. 2014; Sulpizio et al. 2014; Dufek 2016), their motion is mainly controlled by the density contrast with the surrounding atmosphere and topography (Sulpizio and Dellino 2008; Jenkins et al. 2013; Mele et al. 2015). In particular, DPDCs represent the low-particle concentration type of pyroclastic density currents (Valentine 1987; Burgisser and Bergantz 2002; Sulpizio et al. 2007; Dellino et al. 2008; Sulpizio and Dellino 2008; Sulpizio et al. 2014; Breard et al. 2015; Dufek 2016). In a DPDC, while particles are transported mainly by the mechanism of turbulent suspension, inter-particle collisions and fluidization phenomena play a negligible role and are mainly restricted to a thin basal layer (Fig. 1a). On the other hand, in a high-particle concentration type of pyroclastic flows, particle-particle collisions and frictional contacts are the dominant mechanism (Fig. 1a) (Iverson and Vallance 2001; Dellino et al. 2008;

Editorial responsibility: H. Dieterich

Electronic supplementary material The online version of this article (<https://doi.org/10.1007/s00445-017-1191-z>) contains supplementary material, which is available to authorized users.

✉ Fabio Dioguardi
fabiod@bgs.ac.uk

¹ British Geological Survey, The Lyell Centre, Research Avenue South, Edinburgh EH14 4AP, UK
² Dipartimento di Scienze della Terra e Geoambientali, Università degli Studi di Bari "Aldo Moro", Bari, Italy

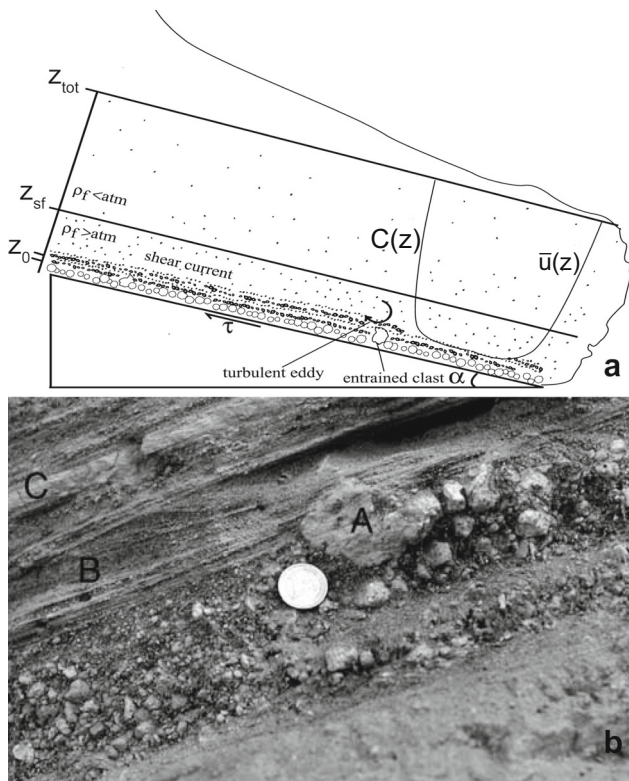


Fig. 1 **a** Scheme of a DPDC deposit on an inclined slope of angle α . The reference level z_0 , the shear flow thickness z_{sf} , and the total flow thickness z_{tot} are shown, together with the concentration profile $C(z)$ and average velocity profile $u(z)$. **b** Picture of a typical complete DPDC deposit, with the layer of coarse lapilli and bombs (A), the laminated layer (B), and the massive thin ash layer (C). Reprinted from *Computer and Geosciences*, 66, Fabio Dioguardi, Pierfrancesco Dellino, *PYFLOW: A computer code for the calculation of the impact parameters of Dilute Pyroclastic Density Currents (DPDC) based on field data.*, 200–210, Copyright (2014), with permission from Elsevier

Sulpizio and Dellino 2008; Roche 2012; Sulpizio et al. 2014; Dufek 2016). Due to their mobility and capability to transport dangerous amounts of hot volcanic ash and gases, DPDCs represent a source of hazard for human life, activities, and infrastructure in the potentially affected areas (Neri et al. 2015a). In particular, their potential impact can be attributed to flow velocity, density, and temperature (Baxter et al. 1998; Neri et al. 2007; Dellino et al. 2008; Caricchi et al. 2014). The dynamic impact of DPDCs on obstacles aligned at right angles to their direction of motion (e.g., walls) is usually quantified by the dynamic pressure, $P_{dyn} = 0.5\rho_f u^2$, where ρ_f is the flow density and u is the velocity along the flow direction. Additionally, DPDCs are also responsible for the transport of ash over long distances, which can be dangerous for people's health even at very low particle volumetric concentration, C (Horwell and Baxter 2006). Finally, forecasting the occurrence, the path, and the potential distance traveled by future DPDCs is currently challenging and subject to significant uncertainties (Neri et al. 2015b), which are further complicated by their ability to delaminate and/or surmount large

topographic obstacles (e.g., Baxter et al. 2005; Charbonnier et al. 2013; Jenkins et al. 2013).

The fluid dynamic behavior of DPDCs in general has been extensively investigated theoretically (e.g., Branney and Kokelaar 2002; Nield and Woods 2003; Doronzo 2012), numerically (e.g., Valentine 1987; Neri et al. 2003, 2007; Esposti Ongaro et al. 2007; Doronzo and Dellino 2011; Bevilacqua et al. 2015; Engwell et al. 2016), and experimentally (e.g., Wilson 1980; Woods and Bursik 1994; Leeder et al. 2005; Dellino et al. 2007, 2010a, b; Roche 2012; Lube et al. 2015; Breard et al. 2016; Sulpizio et al. 2016). However, the analysis of the facies architecture of DPDCs' deposits has also proved to be a powerful tool for understanding the fluid dynamic properties and the sedimentation processes of these flows (e.g., Brown et al. 2007; Sulpizio et al. 2007) and developing "reverse engineering" (Dellino et al. 2008) or inverse modeling approaches, i.e., starting from the result (the deposit) to infer the process (the flow) (Chough and Sohn 1990; Dellino et al. 2000, 2004; Dioguardi and Dellino 2014; Mele et al. 2015). In fact, DPDC deposits are characterized by peculiar properties, in particular concerning their stratigraphy: the typical bedset starts from the base with a layer made of coarse particles (generally lapilli, layer A in Fig. 1b). These particles could be already present on the ground during the passage of the DPDC, or represent particles falling into the flow and that were too coarse to be transported in turbulent suspension. Typically, layer A can be observed in proximal areas (Dellino et al. 2008; Mele et al. 2015). The sequence continues upwards with the main signatures of DPDC deposits, i.e., a level characterized by internal laminations, often with cross lamination and wavy structures, usually composed of ash and fine lapilli (layer B in Fig. 1b). This part is generally attributed to the particles settling from turbulent suspension (Branney and Kokelaar 2002; Dellino et al. 2004, 2008; Sulpizio and Dellino 2008; Sulpizio et al. 2016). A layer of thin massive ash generally closes the sequence on top: this is formed by the fine ash slowly settling in the waning stage of the flow (layer C in Fig. 1b).

From the early 2000s, volcanologists started to work on the development of sedimentological models that linked the deposit architecture and properties described above to the flow characteristics (Dellino and La Volpe 2000; Dellino et al. 2004). In the first pioneering studies, a similarity between DPDCs and turbulent boundary layer shear flows (TBLSF, Furbish 1997; Schlichting and Gersten 2000; Pope 2000), which form when a turbulent fluid moves over a solid boundary, was hypothesized and proven. Subsequent improvements and refinements led to an initial sedimentological model allowing calculation of some of the impact parameters (dynamic pressure and particle volumetric concentration) of DPDCs starting from deposit data (Gurioli et al. 2002; Dellino et al. 2008). The model was later validated by means of large-scale experiments (Dellino et al. 2010b) and

implemented in the first version of PYFLOW in order to simplify and speed up the calculation procedure (Dioguardi and Dellino 2014).

In this paper, a new version of PYFLOW (version 2.0) is presented, together with two applications showing the capabilities of the software. Version 2.0 is significantly improved over the initial version both in terms of the sedimentological modeling (the implementation of different shape-dependent drag laws and of a new model for calculating the deposition rate and time) and in the informatics (with faster numerical routines and a user-friendly input data method). The software and user's manual are given in the electronic supporting material linked to the paper (Electronic Supplementary Material: Folder = PYFLOW_2.0).

Model

In this section, the sedimentological model for calculating flow properties (e.g., bulk density, velocity, and dynamic pressure) is briefly described. A more detailed description, including the computational methods, can be found in the user's manual (Electronic Supplementary Material: PYFLOW_2.0/Manual/Manual.pdf) included in the software package available in the electronic supporting material linked to the paper (Electronic Supplementary Material: Folder = PYFLOW_2.0). The software is also available at <https://vhub.org/resources/4234>. In the following, we will mainly focus on the new modeling features introduced in the code, where all symbols and notations are defined in Table 1.

TBLSF as an approximation of DPDCs

The analogy between TBLSFs and turbulent dilute geophysical surface flows has been proposed for many decades, in particular for the transport and deposition of sediments in particle-laden turbulent flows (Middleton and Southard 1984), and applied in the volcanic context to calculate average velocity and density of DPDCs of some past explosive eruptions at Vulcano, Aeolian Islands (Dellino and La Volpe 2000) and Campi Flegrei (Dellino et al. 2004). A complete sedimentological model based on this analogy was presented in Dellino et al. (2008), experimentally validated in Dellino et al. (2010b) and included in a first preliminary version of the presented software (Dioguardi and Dellino 2014).

In a DPDC, solid particles, which usually show a wide range of size (from fine ash to coarse lapilli) and componentry (pumice, crystals, lithic fragments, etc.), are held in suspension by the effect of the carrier fluid turbulence, since the vertical component of the velocity fluctuations that are directed upward contrasts with the downward particles' settling velocity (Dellino et al. 2008). Indeed, as it follows from Prandtl's assumption (Furbish 1997; Schlichting and Gersten 2000), the

shear stress at the base of the current is $\tau_0 = \rho_f u_*^2 = -\rho_f \overline{u'w'}$, where u_* is the shear velocity and $\overline{u'w'}$ is the covariance of the fluctuating velocities in the stream (x) and upward (z) directions.

A peculiar characteristic of turbulent dilute gravity currents like DPDCs is the vertical particle concentration stratification resulting from the combined action of gravity and the diffusive effect of the gas turbulence over the particles transported in turbulent suspension. The vertical concentration profile was first described by the Rouse equation (Rouse 1939), which quantifies the maximum load of particles (expressed as particle volumetric concentration C) that can be transported in turbulent suspension by a turbulent flow:

$$C(z) = C_0 \left(\frac{z_0}{z_{\text{tot}} - z_0} \frac{z_{\text{tot}} - z}{z} \right)^{P_n} \quad (1)$$

where C_0 is the particle volumetric concentration at the reference level z_0 and z_{tot} is the total flow thickness (Fig. 1a). Here, z_0 is the base level at which the particles are being settled from suspension, i.e., where $C(z)$ approaches the maximum packing limit typical of the very thin bedload at the base of a sediment current (0.75 in Dellino et al. 2008). In this equation, an important role is played by the Rouse number P_n , a dimensionless parameter defined as

$$P_n = \frac{w}{ku_*} \quad (2)$$

where w is the particle settling velocity and k is Von Karman's constant (equal to 0.4). It is straightforward to infer from (2) that P_n describes the tendency of particles to be transported by a turbulent flow. When $P_n > 2.5$, a particle is at settling conditions, whereas when $P_n < 2.5$, it can be held in suspension (Middleton and Southard 1984). In a DPDC, the solid phase is represented by a population of particles, each one characterized by different size, density, drag, hence different settling velocity w . The Rouse number P_n therefore represents an average value of the population of particles transported in the turbulent flow.

The particle concentration profile controls the flow density profile, as it results from the definition of fluid bulk density ρ_f in the multiphase framework:

$$\rho_f(z) = (1 - C(z))\rho_g + C(z)\rho_s \quad (3)$$

where ρ_g and ρ_s are the gas and solid particle density, respectively. Given the vertical density stratification and that the fluid phase is a mixture of hot gas and entrained atmospheric air that is less dense than the surrounding atmosphere (Engwell et al. 2016), DPDCs develop a basal part with a

Table 1 Symbol notation

Symbol	Description	Units
Latin		
A_p	Particle surface area	m^2
A_{sph}	Surface area of the volume equivalent sphere	m^2
c	Circularity	
C	Particle volumetric concentration	
C_d	Drag coefficient	
C_{tot}	Total particle volumetric concentration in the flow	
d	Particle dimension	mm
D_{3D}	3D fractal dimension	
D_l	Particle long axis	m
D_m	Particle intermediate axis	m
D_s	Particle short axis	m
d_{pr}	Equal projected area circle diameter	mm
d_{sph}	Volume equivalent sphere diameter	mm
g	Gravitational acceleration	$m\ s^{-2}$
i	Index identifying the component	
j	Index identifying the grainsize class	
k	Von Karman's constant	
k_s	Roughness of the substrate	m
m	Particle mass	kg
Med_ϕ	Median grainsize	ϕ
N	Total number of grainsize classes in the deposit	
$n_{classes}$	Number of size classes in the grainsize distribution	
n_{comp}	Number of components in the deposit	
P_{dyn}	Dynamic pressure	Pa
P_n	Average Rouse number	
p_s	Weight fraction	
R	Deposition rate	$kg\ m^{-2}\ s^{-1}$
Re	Particle Reynolds number	
Re^*	Particle shear Reynolds number	
t_{dep}	Deposition time	s
u	Flow velocity	$m\ s^{-1}$
u'	Fluctuating velocity in the flow (x) direction	$m\ s^{-1}$
u_*	Shear velocity	$m\ s^{-1}$
w	Particle terminal velocity	$m\ s^{-1}$
w'	Fluctuating velocity in the vertical (z) direction	$m\ s^{-1}$
x	Stream direction	m
z	Vertical direction	m
z_{lam}	Thickness of the laminated layer in the DPDC deposit	m
z_{sf}	Shear flow thickness	m
z_{tot}	Total flow thickness of the DPDC	m
Greek		
α	Slope angle	°
β	Corey shape factor	
γ	Flatness ratio	
η	Gas viscosity	Pa s
θ	Shield parameter	
ρ	Density	$kg\ m^{-3}$
σ_ϕ	Sorting	ϕ
τ	Shear stress	Pa
τ_0	Shear stress at the base of the current	Pa
φ	Sphericity	
φ_{3D}	3D sphericity	
φ_L	Crosswise sphericity	
$\varphi_{ }$	Longwise sphericity	
Ψ	Particle shape factor	
Subscripts		
Symbol	Description	
0	Reference level in the DPDC	
1	Entrained particle	
f	Fluid phase	
g	Gas	
massive	Massive layer	
s	Solid phase (particles)	
sphere	Spherical particle	
susp	Turbulent suspension	
tot	Total	
wash	Wash load	

density greater than the atmospheric density and a top part, which is buoyant (Fig. 1a). The basal portion is the shear current that is responsible for the majority of the dynamic impact of the flow in the direction of motion (dynamic pressure). This is the part of the DPDC that can be described according to the TBLSF theory (Dellino et al. 2008); hence, the time-averaged (over a time interval short enough to capture the main flow field variations but long enough to smooth the velocity fluctuations over) velocity profile of the current can be calculated by the “law of the wall”:

$$\frac{\bar{u}(z)}{u_*} = \frac{1}{k} \ln \frac{z}{k_s} + 8.5 \tag{4}$$

where k_s is the roughness parameter of the substrate, which is proportional to the height of the roughness elements of the substrate (Schlichting and Gersten 2000; Dellino et al. 2008). The top part of the current, which sometimes is also referred to as the co-ignimbrite ash cloud or ash-cloud surge (Branney and Kokelaar 2002), is of high relevance too since it is responsible for the transport of fine ash, which has residence times in the atmosphere that are significantly longer than the particles in the basal part. Additionally, fine ash can have consequences on the health of humans and animals (Horwell and Baxter 2006). Hence, this part needs to be taken into consideration too in order to quantify the whole range of potential impacts of DPDCs, from the lateral impact on building to the fine ash in the atmosphere.

The combination of flow density and velocity profiles leads to the dynamic pressure profile:

$$P_{dyn}(z) = \frac{1}{2} \rho_f(z) \bar{u}(z)^2 \tag{5}$$

which can be spatially averaged over a height (flow thickness) relevant for hazard assessment purposes.

In the dense basal part of the DPDC, particles settle down from suspension and form the bed load. The combination of the stress exerted from the overlying shear flow on the bed load and the continuous sedimentation of particles from suspension results in a progressive aggradation of sediment to form thin traction laminae, which are one of the most distinguishing features of DPDC deposits (Branney and Kokelaar 2002; Sulpizio and Dellino 2008; Dellino et al. 2008). Particles from the overriding dilute portion of the flow, on the other hand, settle during the waning stage of the flow, thus resulting in a fine-grained massive layer that caps the typical stratigraphic sequence that can be attributed to a DPDC.

If the stratigraphic sequence of Fig. 1b is observed in the field and characterized quantitatively in detail by measuring its thickness, grainsize distributions, componentry, particle

density, and shape, it is possible to use PYFLOW to invert deposit data and define the fluid dynamic characteristics of the parent current. The values calculated by PYFLOW represent the flow characteristics at the particular location where the deposit has been recognized in the field. When deposits of the same flow unit of a DPDC are found in different outcrops, the variation of the DPDC behavior and impact in its direction of propagation can be approximated using PYFLOW (Mele et al. 2015). Since the model is based on the TBSF approximation of DPDCs, it is expected to give reasonable results only in the case of dilute turbulent particle-laden currents (Dellino et al. 2008). In some cases, one cannot be completely confident that a deposit in the field is actually the final product of a turbulent DPDC. For this reason, PYFLOW always performs a Student *t* test in the computation stage in order to check the validity of the assumptions in the particular case under investigation.

Based on the observed deposit architecture, it is possible to use two different but complementary approaches for calculating the flow properties using PYFLOW_2.0: the Shield and the suspension-sedimentation criterions.

Shield and suspension-sedimentation criterions

A DPDC can carry particles that are never transported in suspension but that can be moved over the substrate by the current shear stress. Examples can be particles in the flow with $P_n \gg 2.5$ (e.g., coarse particles transported in the proximal locations or falling into the flow from a simultaneous eruptive column) or loose particles on the ground before the DPDC passage. This phenomenon can be quantified by means of the Shield parameter (Miller et al. 1977), which is defined as the ratio between the flow shear stress and the buoyancy force per unit area of the particle in the flow and defines the initiation of motion of particles laying on the substrate:

$$\theta = \frac{\rho_f u_*^2}{(\rho_{s1} - \rho_f) g d_1} \tag{6}$$

where *g* is gravity acceleration and ρ_{s1} and d_1 the density and diameter of the entrained particle, respectively; θ is a parameter depending on the particle shear Reynolds number Re^* ($Re^* = \rho_f u_* d_1 / \eta$ where η is the fluid viscosity), which decreases as Re^* increases (particles are more likely to be moved by the flow) and becomes equal to 0.015 for a Re^* number greater than 1000 (Miller et al. 1977).

On the other hand, at the limit of transportation by turbulent suspension, when $P_n = 2.5$, from (2) and since $k = 0.4$, it follows that

$$w = u_* \tag{7}$$

This is the suspension-sedimentation criterion (Middleton and Southard 1984), which means that particles stay suspended in the flow until their settling velocity is less than the flow shear velocity. In other words, particles in the deposit that settle from suspension (the laminae-forming bed load) give an indication of the flow shear velocity at the time of deposition, once their terminal velocity is defined. Particle settling velocity *w* can be calculated by the so-called Newton impact law (Dellino et al. 2005):

$$w = \sqrt{\frac{4gd(\rho_s - \rho_f)}{3C_d \rho_f}} \tag{8}$$

where *d* is the particle equivalent diameter (i.e., the diameter of the sphere having the same volume of the settling particle) and C_d is the drag coefficient. Upon combining (7) and (8), it follows that

$$u_*^2 = \frac{4gd(\rho_s - \rho_f)}{3C_d \rho_f} \tag{9}$$

The squared shear velocity coincides with the shear stress at the base of the current normalized by the flow density:

$$\tau = \rho_f u_*^2 \tag{10}$$

When the complete stratigraphic sequence described in the previous section is recognized in the field (Fig. 1b), it is possible to apply both the Shield and the suspension-sedimentation criteria for calculating the flow parameters. In PYFLOW, this approach is named “two layers model.” However, the layer of entrained coarse lapilli or bombs, which is typical of proximal locations around the eruptive vent, is often missing in distal outcrops, thus preventing the use of the Shield criterion. In such a case, an alternative method based on the hydraulic equivalence of particles can be used, which in PYFLOW is named the “two components model.” The reader can find details on the two approaches in Dellino et al. (2008), Dioguardi and Dellino (2014), and the user manual provided here (Electronic Supplementary Material: PYFLOW_2.0/Manual/Manual.pdf). In the next sections, we will focus on the new sedimentological models implemented in PYFLOW_2.0.

Necessary input data

In order to use equations (6) through (10) and to solve for the flow shear velocity and density, it is necessary to provide as input, besides layer properties (layer thickness z_{lam} , substrate roughness k_s), the physical properties of the particles representing the laminated layer and possibly the basal coarse

layer. In particular, for the aforementioned two models, the following data are necessary:

- For the “two layers model”: density ρ_{s1} and representative dimension d_1 of the selected particle in the coarse layer; density ρ_s , the representative dimension d , and shape of the particles deposited in the laminated layer; this can be for a selected component (e.g., juvenile glassy particles or crystals).
- For the “two components model”: density ρ_s , representative dimension d , and shape of the particle deposited in the laminated layer of two selected components.

The selection of components for the calculations depends on different factors. As a general guidance, it is advised to select the components based on the relative abundance in the deposit and on the shape of their grainsize distribution, with a unimodal Gaussian distribution to be preferred since it can be interpreted as the result of deposition from turbulent suspension (Dellino et al. 2008). Further details on how to obtain these and other relevant data can be found in the user’s manual (Electronic Supplementary Material: PYFLOW_2.0/Manual/Manual.pdf) and in Dellino et al. (2000, 2004, 2008, 2010b) and Mele et al. (2015).

Shape-dependent drag laws

In the new version presented here, it is possible to choose among nine shape-dependent drag formulas. Volcanic particles cannot be approximated by spheres, especially in the fluid dynamic regimes typical of DPDCs. It is well known, in fact, that the influence of particle shape increases as the particle Reynolds number Re increases (Ganser 1993; Dioguardi et al. 2014; Dioguardi and Mele 2015; Bagheri and Bonadonna 2016; Dioguardi et al. 2017). Therefore, in order to obtain realistic estimates of DPDC impact parameters, it is essential to use shape-dependent drag formulas. These drag formulas are generally a function of Re and one or more particle shape descriptors. Table 2 summarizes the possible choices, the needed shape descriptors, the appropriate reference, and the drag law equations. If the user desires, the code allows calculating the drag assuming spherical particles; in this case, the drag is calculated by using the formula of Clift and Gauvin (1971). The drag law selection can significantly influence the solution, as will be shown in the application examples. This is due to the fact that the sedimentological model is highly sensitive to the variations of the calculated fluid-particle drag. Therefore, we recommend running PYFLOW selecting different drag laws based on the available shape descriptors (e.g., Dellino et al. (2005) and Dioguardi and Mele (2015) if the value of the shape factor Ψ is known).

Particle density and grainsize

In this new version, PYFLOW offers greater flexibility when providing particle density in the laminated layer. In this model, the deposition rates of each grainsize class of each component constituting the deposit, which are directly proportional to particle density (11), are calculated and then summed to obtain the total deposition rate. For juvenile vesiculated particles, density can change significantly with size (Houghton and Wilson (1989); Dellino et al. (2005); Beckett et al. (2015)). Hence, in this new version, PYFLOW offers the possibility to either specify a constant or a size-dependent density, in the latter case either by indicating the density of each grainsize class or using built-in density-versus-size functions, which were obtained by available data from previous studies (e.g., Dellino et al. 2008). Table 3 gives the available size-dependent density laws, while commands for activating them are presented in the user manual (Electronic Supplementary Material: PYFLOW_2.0/Manual/Manual.pdf).

Additionally, PYFLOW can automatically perform grainsize distribution analysis for the two components used in the sedimentological model in order to calculate the median Md_ϕ and sorting σ_ϕ . Optionally, a χ^2 test for checking if the distributions are significantly different from normal Gaussian distribution can be performed. If the depositional model is also activated, the program will perform grainsize analysis by default for all the components considered for this model, since the user will be forced to provide grainsize and density distribution data.

Deposition model

The deposition model calculates the deposition rate and time from the DPDC based on the flow (e.g., flow density, shear velocity, etc.) and deposit properties (componentry, grainsize distributions, etc.). Flow properties required to execute the deposition model (namely density ρ_f , thickness z_{tot} , shear velocity u_*) can either come from the solution of the sedimentological model presented above or be provided in input. The deposition model, in fact, can run as a standalone program provided all the needed flow and particle properties are given in input.

In this model, by neglecting the possible effect of resuspension and/or erosion, the deposition rate R of the j th grainsize class of a component i forming the deposit is given by (Stow and Bowen 1980)

$$R_{i,j} = \rho_{s,i,j} w_{i,j} C_{i,j} \quad (11)$$

where $C_{i,j}$ is the particle volumetric concentration of each grainsize class j in the flow. Since particle density $\rho_{s,i,j}$ is an

Table 2 List of shape-dependent drag laws available in PYFLOW_2.0. The indexes i and j refer to the component and the grainsize class, respectively

Reference	Shape descriptor	Equation
Clift and Gauvin (1971)	Perfect sphere	$C_d = C_{d,sphere} = \frac{24}{Re} [1 + 0.15Re^{0.687}] + \frac{0.42}{1 + \frac{32500}{Re^{1.16}}}$
Haider and Levenspiel (1989)	Sphericity φ	$C_d = \frac{24}{Re} (1 + ARe^B) + \frac{C}{1 + \frac{A}{Re}} A = \exp(2.329 - 6.458\varphi + 2.449\varphi^2)$
Swamee and Ojha (1991)	Corey shape factor β	$B = 0.0964 + 0.5565\varphi$ $C = \exp(4.905 - 13.894\varphi + 18.422\varphi^2 - 10.26\varphi^3)$ $D = \exp(1.468 - 12.258\varphi + 20.732\varphi^2 - 15.886\varphi^3)$ $C_d = \left\{ \frac{48.5}{(1 + 4.5\beta^{0.35})^{0.8} Re^{0.64}} + \left[(\frac{Re}{Re} + 100 + 100\beta)^{0.32} \frac{1}{\beta^{18 + 1.05\beta^{0.8}}} \right] \right\}$
Ganser (1993)	Isometric particle Non-isometric particle	Sphericity φ Sphericity φ Volume equivalent sphere diameter d_{sph} Circle equivalent sphere diameter d_{pr} $C_d = \frac{24}{ReK_1K_2} [1 + 0.1118(ReK_1K_2)^{0.6567}] + \frac{0.4305}{1 + \frac{3305}{ReK_1K_2}}$ $K_1 = \begin{cases} \left[\frac{1}{3} + \left(\frac{2}{3}\right)\varphi^{-0.5} \right]^{-0.1} & \text{isometric shapes} \\ \left[\frac{d_{sph}}{3d_{pr}} + \left(\frac{2}{3}\right)\varphi^{-0.5} \right]^{-0.1} & \text{non-isometric shapes} \end{cases}$ $K_2 = 10^{1.8148(-\log\varphi)^{0.5743}}$
Chien (1994)	Sphericity φ	$C_d = \frac{30}{Re} + 67.289e^{-5.03\varphi}$
Tran-Cong et al. (2004)	Circularity c Flatness ratio γ	$C_d = \frac{24}{Re} \gamma \left[1 + \frac{0.15}{\sqrt{c}} (\gamma Re)^{0.687} \right] + \frac{0.42\gamma^2}{\sqrt{c} [1 + 4.25 \times 10^4 (\gamma Re)^{-1.16}]}$
Dellino et al. (2005)	Shape factor Ψ	$C_d = \frac{0.9297}{\Psi^{1.6} Re^{0.0799}}$
Hölzer and Sommerfeld (2008)	Sphericity φ Longwise sphericity $\varphi_{ }$ Crosswise sphericity φ_{\perp}	$C_d = \frac{8}{Re} \frac{1}{\sqrt{\varphi_{ }}} + \frac{16}{Re} \frac{1}{\sqrt{\varphi}} + \frac{3}{\sqrt{Re}} \frac{1}{\varphi^{0.75}} + 0.4210^{0.4(-\log\varphi)^{0.2}} \frac{1}{\varphi_{\perp}}$
Dioguardi and Mele (2015)	Shape factor Ψ	$C_d = \frac{C_{d,sphere}}{Re^2 \Psi Re^{-0.23}} \left(\frac{Re}{1.1883} \right)^{\frac{1}{0.4826}}, Re < 50$ $C_d = \frac{C_{d,sphere}}{Re^2 \Psi Re^{0.05}} \left(\frac{Re}{1.1883} \right)^{\frac{1}{0.4826}}, Re > 50$
Dioguardi et al. (2017)	3D fractal dimension D_{3D} 3D sphericity φ_{3D}	$C_d = \frac{4}{3} \frac{0.3492 C_{d,sphere} (Re^{1.62} D_{3D} Re^{-0.13})^{1.3358}}{Re^2}$ $C_d = \frac{4}{3} \frac{0.559 C_{d,sphere} (Re^{4.18} \varphi_{3D}^{-Re^{-0.2}})^{0.5134}}{Re^2}$

input parameter and the terminal velocity w_{ij} can be readily calculated from (8), C_{ij} needs to be evaluated at this stage. To do so, it is assumed that the ratio between the sedimentation rates of the j th and $j + 1$ th classes in the flow, taking all the $N = \sum_{i=1}^{n_{comp}} n_{classes,i}$ grainsize classes in the deposit together (n_{comp} is the number of components constituting the deposit and considered in the calculation, $n_{classes}$ is the number of grainsize

classes for each component), is equal to the ratio of the weight fractions p_s of the same classes in the deposit formed by that flow:

$$\frac{p_{s,j}}{p_{s,j+1}} = \frac{R_j}{R_{j+1}} = \frac{\rho_{s,j} w_j C_j}{\rho_{s,j+1} w_{j+1} C_{j+1}} \tag{12}$$

Table 3 List of available empirical laws for calculating the size-dependent density of juvenile vesiculated particles

Eruption	Equation	Limiting value	Reference
Pollena	$\rho_s = 1000(-0.31 \log d + 1.83)$	2760 kg m ⁻³	Dellino et al. (2008)
Averno	$\rho_s = 1000(-0.3 \log d + 1.42)$	2600 kg m ⁻³	Dellino et al. (2008)
Agnano Monte Spina	$\rho_s = 1000(1.06d^{-0.332})$	2560 kg m ⁻³	Unpublished data
Pompeii	$\rho_s = 1000(1.822d^{-0.167})$	2700 kg m ⁻³	Unpublished data
Mercato	$\rho_s = 1000(0.956d^{-0.191})$	2400 kg m ⁻³	L'Abbate (2007)
Astroni	$\rho_s = 1000(0.812d^{-0.213})$	2510 kg m ⁻³	Manzaro (2005)

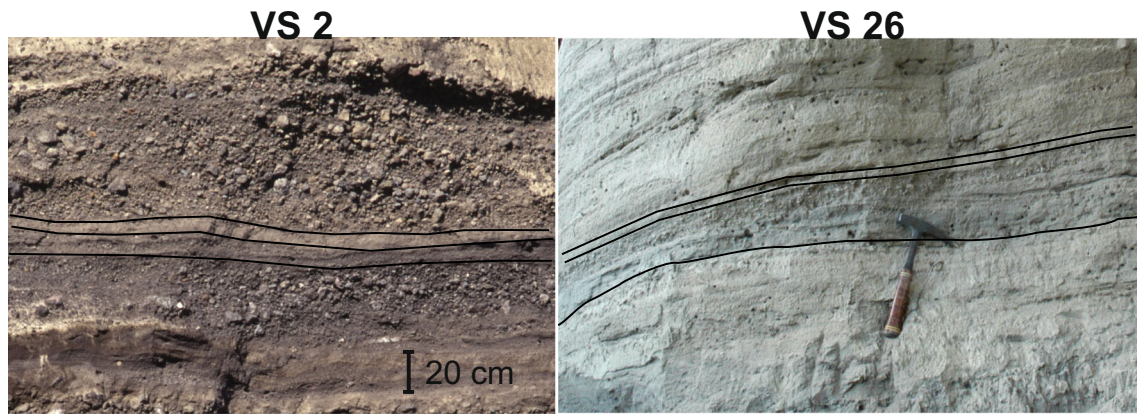


Fig. 2 Photos of the outcrops used for the application examples. Left picture: Pollena VS2. Right picture: Pollena VS26 (hammer length:

28 cm). The black solid lines delimit the outcrop area sampled for the calculations

This equation is solved for each grainsize class, thus forming a system of N equations:

$$\begin{cases} C_j = \frac{P_{s,j}\rho_{s,j+1}W_{j+1}C_{j+1}}{P_{s,j+1}\rho_{s,j}W_j} \\ C_{j+1} = \frac{P_{s,j+1}\rho_{s,j+2}W_{j+2}C_{j+2}}{P_{s,j+2}\rho_{s,j+1}W_{j+1}} \\ \vdots \\ C_{N-1} = \frac{P_{s,N-1}\rho_{s,N}W_N C_N}{P_{s,N}\rho_{s,N-1}W_{N-1}} \\ C_N = C_{tot} - \sum_{j=1}^{N-1} C_j \end{cases} \quad (13)$$

where C_{tot} is the total particle volumetric concentration in the flow. This is obtained by the bulk flow density ρ_f and weight-averaging the particle density of all the grainsize classes:

$$C_{tot} = \frac{\rho_f - \rho_g}{\sum_{j=1}^N \rho_{s,j} P_{s,j}} \quad (14)$$

In this model, particles are classified as either constituting the turbulent suspension or the wash load categories based on their Rouse number $P_{n,i,j}$ (Rouse 1939; Middleton and Southard 1984):

- Wash-load: $P_{n,i,j} < 0.8$
- Turbulent suspension: $0.8 < P_{n,i,j} < 5.0$
- Fall: $P_{n,i,j} > 5.0$

Particles whose Rouse number is less than 0.8 constitute the wash load, i.e., particles that are uniformly distributed throughout the flow and mainly settle in the waning stage of the flow. If a fine massive layer is observed in the deposit (level C in Fig. 1b), PYFLOW can calculate the deposition rate and time contributions of this layer if the layer thickness is provided ($z_{lam, massive}$). In the current

version, PYFLOW automatically assumes this layer is formed by particles of the laminated layer that can be attributed to the wash-load ($P_{n,i,i} < 0.8$). For these particles, the volumetric concentration is calculated by multiplying their weight fraction with the ratio between the fine massive layer thickness and the flow thickness. If a grainsize and componentry analysis of this specific layer is carried out, it is possible to calculate the deposition rate and time of this layer separately thanks to the capability of PYFLOW to run this module as a standalone. Additionally, particles with a Rouse number greater than five can be optionally discarded, since these particles can be considered to fall in the deposit without being influenced by the turbulent flow. This threshold is approximate, but important for excluding these particles from the calculation to prevent an overestimation of the deposition rate and an underestimation of the deposition time. We choose the critical value of five as a safe approximation, which is double the value of 2.5 that describes when

Table 4 Input parameters and corresponding commands of the Pollena 2-3 application example

Input variable	Value
Gas viscosity (η)	$2 * 10^{-5}$ Pa s
Gas density (ρ_g)	0.38 kg m^{-3}
Layer thickness (z_{lam})	0.2 m
Concentration at the reference level (C_0)	0.75
Substrate roughness (k_s)	0.04 m
Entrained particle density (ρ_{s1})	2570 kg m^{-3}
Entrained particle dimension (d_1)	0.08 m
Component 1 density (ρ_s)	1750 kg m^{-3}
Component 1 median grainsize (d)	1.286 mm
Component 1 sorting (σ_φ)	1.54
Component 1 number of grainsize classes ($n_{classes}$)	17
Selected drag law for component 1	Dellino et al. (2005)
Component 1 shape factor (Ψ)	0.47

particles start to settle in the turbulent DPDC (since $w = u_*$) to form the bedload (Rouse 1939; Middleton and Southard 1984). PYFLOW2.0 allows the user to avoid this cutoff or change this critical value. After the system of equations given in (13) has been solved for the particle concentrations C_j (details on the calculation procedure are neglected here; the reader can refer to the supplied user manual (Electronic Supplementary Material: PYFLOW_2.0/Manual/Manual.pdf)), the total deposition rate and time of both the laminated layer and the fine massive layer (if present and/or considered) are calculated:

$$R_{tot,susp} = \sum_{i=1}^{n_{comp}} \sum_{j=j_{wash,i}+1}^{n_{classes,i}} \rho_{s,i,j} W_{i,j} C_{i,j} = \sum_{i=1}^{n_{comp}} \sum_{j=j_{wash}+1}^{n_{classes,i}} R_{i,j,susp} \quad (15)$$

$$R_{tot,massive} = \sum_{i=1}^{n_{comp}} \sum_{j=1}^{j_{wash,i}} \rho_{s,i,j} W_{i,j} C_{i,j} = \sum_{i=1}^{n_{comp}} \sum_{j=1}^{j_{wash,i}} R_{i,j,massive} \quad (16)$$

$$R_{tot} = R_{tot,susp} + R_{tot,massive} \quad (17)$$

$$t_{dep,susp} = \frac{z_{lam,susp} C_0 \sum_{i=1}^{n_{comp}} \sum_{j=j_{wash,i}+1}^{n_{classes,i}} \rho_{s,i,j} P_{s,i,j}}{R_{tot,susp}} \quad (18)$$

$$t_{dep,massive} = \frac{z_{lam,massive} C_0 \sum_{i=1}^{n_{comp}} \sum_{j=1}^{j_{wash,i}} \rho_{s,i,j} P_{s,i,j}}{R_{tot,massive}} \quad (19)$$

$$t_{dep,tot} = t_{dep,susp} + t_{dep,massive} \quad (20)$$

where $j_{wash,i}$ is the index of the coarsest grainsize class constituting the wash load of the component i and the subscripts *susp* and *massive* refer to the laminated and the fine massive layer, respectively.

For the total deposition rate R_{tot} and deposition time $t_{dep,tot}$, the average, maximum, and minimum solutions are calculated, since R_{tot} (and hence $t_{dep,tot}$) depends on the flow bulk density, for which the three solutions were calculated in the previous steps.

Application examples

Two application examples are described in this section. The test cases are designed to cover the largest possible range of applications and commands. It is straightforward to run other cases by simply amending the input files of the provided test cases (Electronic Supplementary Material: Folder = PYFLOW_2.0/Test_cases).

The application examples build on field data collected from laminated pyroclastic density current deposits of the Pollena Subplinian eruption (AD 472; Vesuvius, Italy). In particular, we examined deposits of S2 (sample vs 2_3)

and S3 units (sample vs 26_1), which were emplaced by a dilute pyroclastic current during the second and third phase of the eruption, respectively (Sulpizio et al. 2005; 2007). Their deposits consist of ash with lenses of lapilli that form low-amplitude, meter-spaced dunes with internal cross stratification (Fig. 2). At a few locations, the deposits show the bedset that reflects the fining upward sequence described in Fig. 1b. From the bottom, the outcrops start with a basal layer made of inversely graded coarse lapilli presenting a preferential orientation that can be attributed to the overlying flow. This layer is followed by a laminated layer with cross stratification of fine lapilli/coarse ash and finally topped by a massive fine-ash layer.

The input and result files can be found in the folders “Pollena/2-3” and “Pollena/26-1” (Electronic Supplementary Material: Folder = PYFLOW_2.0/Test_cases). Details on the field and laboratory analyses carried out for obtaining input parameters can be found in the Electronic Supplementary Material (PYFLOW_2.0/Sampling and laboratory analyses.docx).

Pollena VS2-3

In this case, we use the “two layers” method described previously. Detailed explanations on how to create the input file are provided in the user manual, where the same test cases are described (Electronic Supplementary Material: Folder = PYFLOW_2.0/Manual/Manual.pdf).

From the basal layer (A in Fig. 1b), we selected a particle with a diameter of 0.08 m and a density of 2570 kg m⁻³. From the laminated layer (B in Fig. 1b), we selected the juvenile particles (median grainsize and density 1.286 mm and 1750 kg m⁻³, respectively). In Table 4, input data for the physical variables needed in the calculation are summarized together with the corresponding entries in the input file.

Results of this test case are summarized in results.dat (Electronic Supplementary Material: Folder = Test_cases/Pollena/2-3), whose screenshots are shown in the user manual (Electronic Supplementary Material: PYFLOW_2.0/Manual/Manual.pdf). The file is organized as follows: in the first part (“Data summary”), input data for the sedimentological model (Table 4) are summarized for both components; results for the main flow properties (average, maximum, and minimum solutions) are subsequently written, followed by a summary of the Student t test. The file continues with all the user-requested outputs, in this case the average specific dynamic pressure at 5 and 2 m height from the base of the current. The following section contains results from the probability density function routine (symmetrization exponent, median μ_{simmm} and standard deviation σ_{simmm}) for all the considered impact parameters and

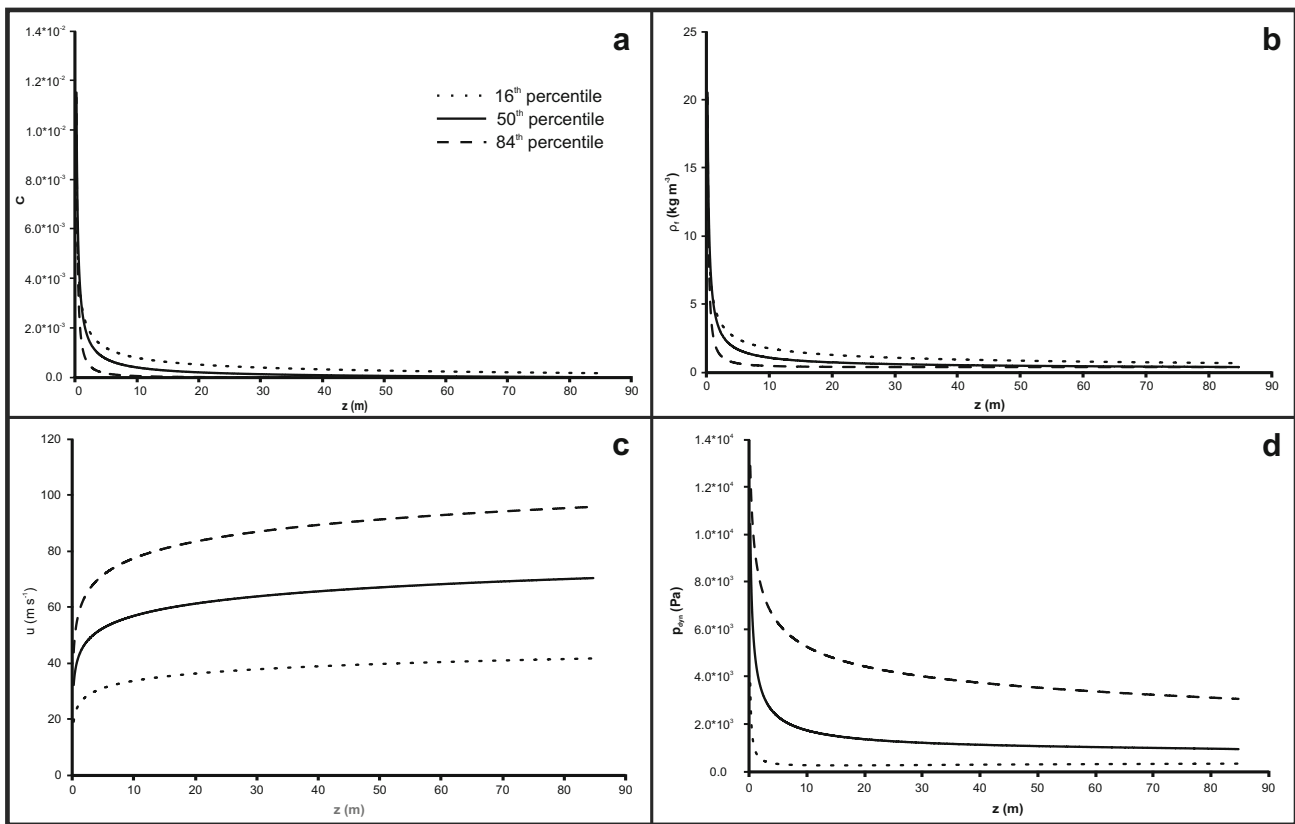


Fig. 3 Plots of the vertical profiles of the calculated flow field variables for the Pollena VS2-3 application example. Dotted, solid, and dashed black lines represent the solutions at 16th percentile, 50th percentile,

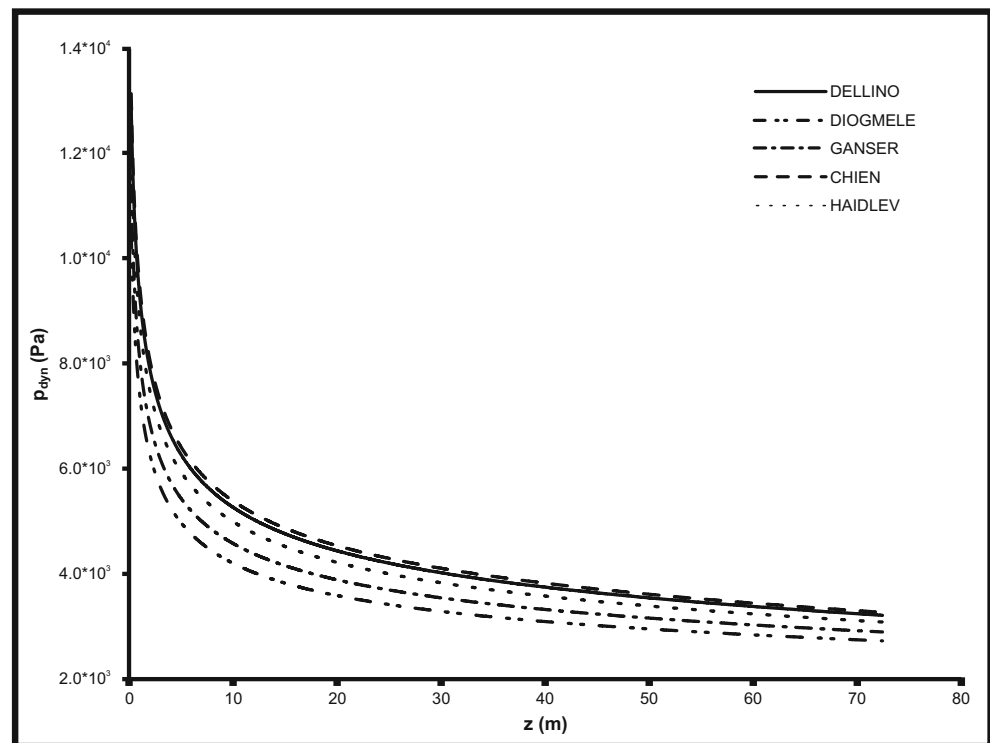
and 84th percentile, respectively. **a** Particle volumetric concentration C . **b** Flow density ρ_f . **c** Flow velocity u . **d** Flow dynamic pressure P_{dyn}

the values of the impact parameters at the user-requested percentile.

Figure 3 shows plots of the vertical profiles of the flow variables as plotted by opening the files `conc_profile.dat`, `dens_profile.dat`, `vel_profile.dat`, `pdyn_profile.dat` (Electronic Supplementary Material: Folder = Test_cases/Pollena/2-3/main) with Excel. The calculated flow properties are typical of a DPDC that could exert a significant impact, with an average dynamic pressure over the first 10 m of 3 kPa, which becomes 4.15 kPa over the first 5 m and 6.2 kPa over the first 2 m. These values of dynamic pressure can potentially cause damage that can be classified as moderate to heavy (Baxter et al. 2005), mainly consisting of the failure of doors and windows. If one considers the maximum solution with an exceedance probability of 5%, calculated values significantly increase reaching 12.1 kPa over the first 2 m height, a value that can potentially cause heavy damage to partial devastation (Baxter et al. 2005), with walls starting to be affected. This reflects the strong vertical stratification of these currents, which can be further appreciated by looking at the profiles of Fig. 3. The particle concentration, hence flow density, shows particularly steep gradients which, combined with the gentler velocity gradient, results in a parabolic-like dynamic pressure vertical profile.

Finally, we analyze the influence of the shape-dependent drag laws on the solution (Electronic Supplementary Material: Folder = Test_cases/Pollena/2-3/drag_laws). For the examined deposit, in particular for the juvenile component taken under consideration, particle sphericity φ is available alongside the shape factor Ψ : 0.727. This allowed performing the calculation with five different drag laws: Dellino et al. (2005) and Dioguardi and Mele (2015) (shape factor Ψ); Haider and Levenspiel (1989), Ganser (1993), and Chien (1994) (sphericity φ). Figure 4 shows the vertical profile of dynamic pressure corresponding to the maximum solution as calculated by PYFLOW by default (16% exceedance probability) for the five considered drag laws. The curves follow the same trend, but some differences can be noted, with the laws of Chien (1994) and Dellino et al. (2005) generating the maximum values, while with Dioguardi and Mele (2015) and Ganser (1993) dynamic pressure values are the lowest; finally, the solution with Haider and Levenspiel (1989) lies between the other four curves. Although the difference between the calculated values is not very high, it is not negligible (maximum values about 15%) meaning that, if different shape descriptors are available, it is recommended to run PYFLOW with as many drag laws as possible and to assign an uncertainty (range of variation) to the solution. The influence of the selected drag

Fig. 4 Eighty-fourth percentile solution of dynamic pressure P_{dyn} of Pollena VS2-3 application example calculated with different shape-dependent fluid-particle drag laws. Solid line: Dellino et al. (2005). Dashed-double-dotted line: Dioguardi and Mele (2015). Dashed-dotted: Ganser (1993). Dashed line: Chien (1994). Dotted line: Haider and Levenspiel (1989)



law becomes even more evident when calculating the deposition rates and times, as discussed in the next section.

Pollena VS26-1

In this case, the “two components” method was used in conjunction with the depositional model. Table 5 summarizes the input data relevant for running the two components model. A screenshot of the results.dat (Electronic Supplementary Material: Folder = Test_cases/Pollena/26-1/main) file is shown in the user manual (Electronic Supplementary Material: PYFLOW_2.0/Manual/Manual.pdf), in particular the section related to the deposition rate and time calculations. Since, as already stated, the deposition model can run as standalone, the user can run it for up to six separate simulations with different input flow field parameters, results are then organized under headers identifying the solution number without the attributes “average,” “maximum,” or “minimum.” In this example, PYFLOW calculated the three solutions by default starting from the three flow solutions of the “two components” model; in particular, “solution 1” corresponds with the average, “solution 2” with the maximum (84th percentile), and “solution 3” with the minimum (16th percentile) solution. The deposition rate is minimum at solution 2 ($\sim 0.85 \text{ kg m}^{-2} \text{ s}^{-1}$), since it strongly depends on the flow density, which is minimum at the 84th percentile solution of the sedimentological model. It follows that the deposition time takes its maximum value at this percentile ($\sim 1250 \text{ s}$, corresponding to 21 min) and ranges from few to 21 min, values that are

compatible with other pyroclastic flows that were directly observed (e.g., Brand et al. 2016). The deposition time corresponds to the time in which volcanic ash is in the air settling from the turbulent basal part and the co-ignimbrite ash cloud in the waning stage and can be potentially inhaled by human beings and animals. In Fig. 5, the deposition rates of all the grainsize classes for all the four components (vesiculated juveniles, pyroxenes, lithic fragments, and sialic crystals) are displayed as a function of the grainsize for each solution. These plots were drawn by opening the file deposition_summary.dat (Electronic Supplementary Material: Folder = Test_cases/Pollena/26-1/main) with Microsoft Excel, which includes also the grainsize, terminal velocity, Rouse number, particle density, and volumetric concentration for all the components and all the solutions. The deposition rates of the grainsize classes unavoidably reflect the grainsize distribution in the deposit. This can be further verified by comparing the curves with the histograms in Fig. 6, in which the grainsize distributions for all the components for solution 1 are shown. Note that the grainsize distributions are cut towards the coarsest grainsizes; this is the result of PYFLOW neglecting the particles with $P_n > 5$. In this test case (Electronic Supplementary Material: Folder = Test_cases/Pollena/26-1/no_pn-cut), grainsize distribution is characterized by relatively low fractions of coarse particles with $P_n > 5$; this results in very similar values of deposition rates (range $0.867\text{--}5.38 \text{ kg m}^{-2} \text{ s}^{-1}$) and times (range 201–1250 s) calculated if these particles are not discarded from the calculation.

Table 5 Input parameters and corresponding commands of the Pollena 26-1 application example (only input data for the two components model are shown)

Input variable	Value
Gas viscosity (η)	$2 \cdot 10^{-5}$ Pa s
Gas density (ρ_g)	0.38 kg m^{-3}
Layer thickness (z_{lam})	0.58 m
Concentration at the reference level (C_0)	0.75
Substrate roughness (k_s)	0.01 m
Component 1 density ($\rho_{s,\text{juv}}$)	Variable density
Component 1 median grainsize (d_{juv})	Calculated by grainsize analysis
Component 1 sorting (σ_φ)	Calculated by grainsize analysis
Component 1 number of grainsize classes (n_{classes})	Calculated by grainsize analysis
Selected drag law for component 1	Dioguardi and Mele (2015)
Component 1 shape factor (Ψ)	0.52
Component 1 sphericity (φ)	0.727
Component 2 density (ρ_s)	2570 kg m^{-3}
Component 2 median grainsize (d)	Calculated by grainsize analysis
Component 2 sorting (σ_φ)	Calculated by grainsize analysis
Component 2 number of grainsize classes (n_{classes})	Calculated by grainsize analysis
Selected drag law for component 2	Dioguardi and Mele (2015)
Component 2 shape factor (Ψ)	0.4
Component 2 sphericity (φ)	0.615
Component 3 density (ρ_s)	3280 kg m^{-3}
Component 3 median grainsize (d)	Calculated by grainsize analysis
Component 3 sorting (σ_φ)	Calculated by grainsize analysis
Component 3 number of grainsize classes (n_{classes})	Calculated by grainsize analysis
Selected drag law for component 3	Dioguardi and Mele (2015)
Component 3 shape factor (Ψ)	0.61
Component 3 sphericity (φ)	0.791
Component 4 density (ρ_s)	2400 kg m^{-3}
Component 4 median grainsize (d)	Calculated by grainsize analysis
Component 4 sorting (σ_φ)	Calculated by grainsize analysis
Component 4 number of grainsize classes (n_{classes})	Calculated by grainsize analysis
Selected drag law for component 4	Dioguardi and Mele (2015)
Component 4 shape factor (Ψ)	0.65
Component 4 sphericity (φ)	0.799

Finally, in order to show the sensitivity of model results to the chosen drag law and changes of particle shape descriptors, we run this simulation first by fixing the drag law (Dioguardi and Mele 2015) and changing the value of the shape factor for all the components (Electronic Supplementary Material: Folder = Test_cases/Pollena/26-1/sensitivity_shape-factor) and then by using the original input data and changing the drag laws (Electronic Supplementary Material: Folder = Test_cases/Pollena/26-1/sensitivity_drag-law). Results from this analysis are listed in the Excel file “sensitivity_results.xlsx” ((Electronic Supplementary Material: Folder = Test_cases/Pollena/26-1). For the former test, the shape factor was varied ± 5 and $\pm 10\%$ (over the possible range of variation of the shape factor 0–1), hence resulting in four additional simulations. For the latter test, we run four additional simulations by using other drag laws, namely Dellino et al. (2005), Haider and Levenspiel (1989),

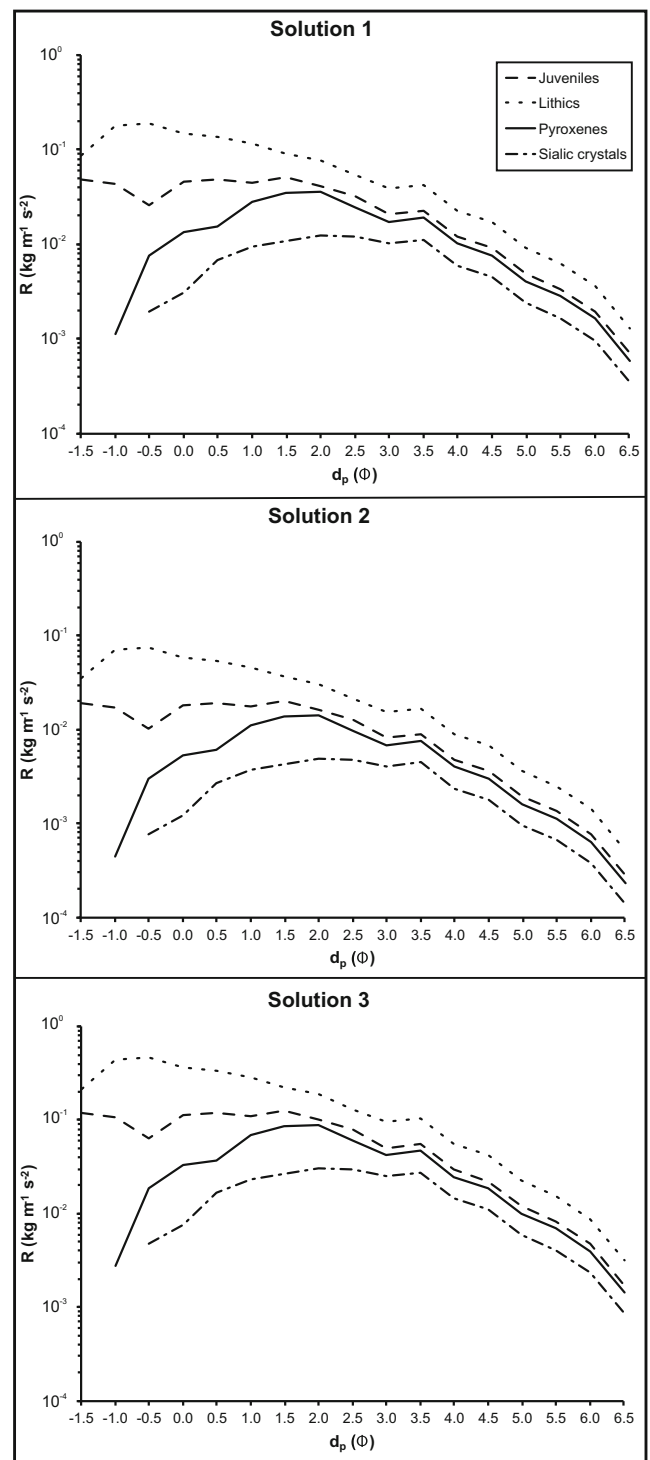


Fig. 5 Plots showing the deposition rate vs. particle size for the four components (dashed line: juvenile particles; solid line: pyroxenes; dotted line: lithic fragments; solid-dotted line: sialic crystals) of the Pollena 26-1 deposit. Solution 1, 2, and 3 correspond to the average, maximum, and minimum solution of PYFLOW, respectively

Ganser (1993), and Chien (1994). These drag laws were selected since they depend on shape descriptors (shape factor Ψ and sphericity φ) that were available for this test case (see Table 5).

Fig. 6 Histogram showing the grainsize distribution of the four components (dark grey: juvenile particles; black: pyroxenes; white: lithic fragments; light grey: sialic crystals) of the Pollena 26-1 deposit

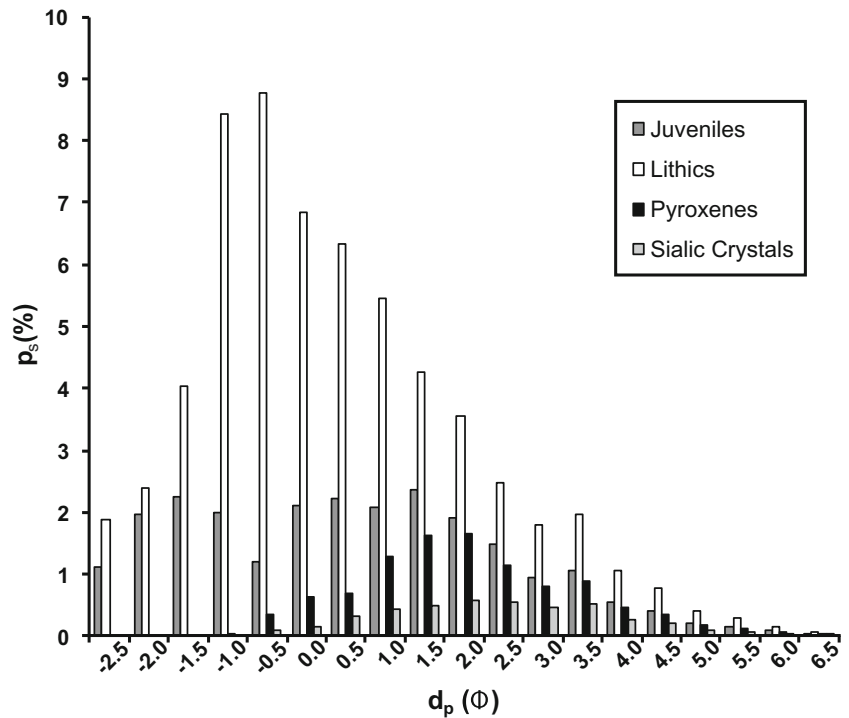


Table 6 Results of the analysis of the sensitivity of PYFLOW_2.0 to the shape factor Ψ variation and the selection of the different shape-dependent drag laws

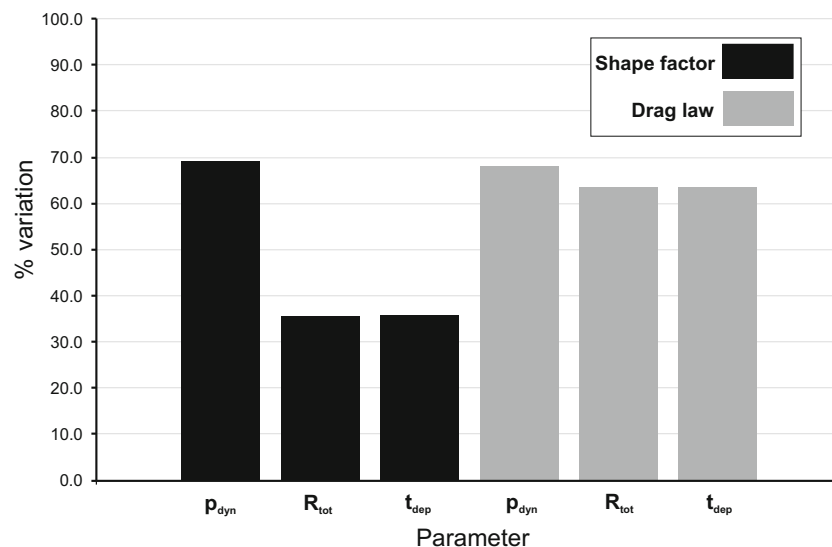
Variable	Max	Min	Range	% variation
Sensitivity to shape factor variation				
P_{dyn} 50th percentile (Pa)	1277.2	393.4	883.8	69.2
P_{dyn} 84th percentile (Pa)	5093.7	2031.4	3062.3	60.1
P_{dyn} 16th percentile (Pa)	289.3	98.7	190.7	65.9
R_{tot} 50th percentile (kg m ⁻² s ⁻¹)	2.5	1.6	0.9	35.6
R_{tot} 84th percentile (kg m ⁻² s ⁻¹)	0.9	0.7	0.2	21.6
R_{tot} 16th percentile (kg m ⁻² s ⁻¹)	6.5	4.2	2.3	35.7
t_{dep} 50th percentile (s)	660.0	424.0	236.0	35.8
t_{dep} 84th percentile (s)	1590.0	1250.0	340.0	21.4
t_{dep} 16th percentile (s)	256.0	165.0	91.0	35.5
Sensitivity to drag law selection				
P_{dyn} 50th percentile (Pa)	776.4	248.1	528.4	68.0
P_{dyn} 84th percentile (Pa)	3428.2	1666.4	1761.8	51.4
P_{dyn} 16th percentile (Pa)	182.4	70.8	111.5	61.2
R_{tot} 50th percentile (kg m ⁻² s ⁻¹)	5.9	2.2	3.8	63.7
R_{tot} 84th percentile (kg m ⁻² s ⁻¹)	3.2	0.9	2.4	73.5
R_{tot} 16th percentile (kg m ⁻² s ⁻¹)	10.3	5.4	5.0	48.1
t_{dep} 50th percentile (s)	493.0	179.0	314.0	63.7
t_{dep} 84th percentile (s)	1250.0	329.0	921.0	73.7
t_{dep} 16th percentile (s)	201.0	103.0	98.0	48.8

Results are summarized in Table 6 and Fig. 7, the latter showing range of variation of the 50th percentile solutions only, to which we refer in the following. Results of the test on the shape factor variation (black bars in Fig. 7) show that, for an overall variation of the shape factor of 20% around the original values (which is quite a wide range of uncertainty for this shape descriptors; see Dellino et al. 2005 and Dioguardi and Mele 2015), the calculated dynamic pressures varied by ~65%, while deposition rates and times varied by ~30%. Deposition rates are less sensitive, but still the influence of the shape descriptor on the deposition rate and time is relatively high, since it directly affects the particle terminal velocity. Deposition rates are instead significantly more sensitive to the chosen drag law, with absolute range of variations of the different solutions of deposition rate and time between ~50 and ~73% (Fig. 7). This is not surprising, since terminal velocities are strongly dependent on the fluid-particle drag C_d (8), which, in turn, changes significantly with the selected drag model. Results of the sensitivity tests confirm that it is recommended to run the model with different drag laws, if the needed shape parameters are available, in particular when calculating the deposition rate and time.

Conclusions and future developments

In this paper, a new software for the quantification of the impact of dilute pyroclastic density currents based on field analysis data (e.g., grainsize, componentry, deposit thickness, etc.) is presented. The software is based on a first preliminary

Fig. 7 Bar plot showing the range of variation of the solved parameters (p_{dyn} , R_{tot} , and t_{dep}) at 50th percentile from the sensitivity analysis of the shape factor Ψ and the drag laws. Black bars: results from the shape factor Ψ sensitivity analysis. Grey bars: results from the drag laws sensitivity analysis



version of PYFLOW presented in the past few years, but it includes significant advances in both the functionalities and the physics. In particular, a new tool has been included for quantifying the deposition rate and time of the flow, hence providing a way to estimate the volcanic ash residence time in the air, which can have a significant impact on potentially exposed human beings and animals. The software is available in the electronic supporting material linked to the paper (Electronic Supplementary Material: Folder = PYFLOW_2.0) and comes with a detailed user manual (Electronic Supplementary Material: PYFLOW_2.0/Manual/Manual.pdf) and two meaningful test cases (Electronic Supplementary Material: Folder = PYFLOW_2.0/Test_cases) based on real data coming from PDC deposits of the Pollena eruption (Vesuvius, Italy), whose results are discussed in this paper. Results from the test case dedicated to the new deposition rate model demonstrate how even relatively weak (i.e., low dynamic pressure) pyroclastic density currents can have a significant impact on people's health given the computed long deposition time (minutes to tens of minutes).

The program is in continuous development and minor modifications and additions are already planned and underway and these updates will be posted on VHUB and linked to this paper (<https://vhub.org/resources/4234>). Potential major modifications will consist of linking the PYFLOW output, which refers to a specific location along the runout path of a past DPDC, to a simplified 1D pyroclastic flow model. In particular, the flow field variables calculated by PYFLOW (vertical profiles of flow velocity and density) can be used as boundary conditions of 1D steady models (e.g., Bursik and Woods 1996), which can be run to obtain a continuous spatial evolution of the flow properties based on realistic boundary conditions. An example of a possible application of this capability could be the evaluation of the spatial evolution of

the flow between two or more discrete points where the flow variables are computed by PYFLOW. This, coupled to a method to interpolate values of flow variables along different runout paths, has the potential to result in a new tool to create impact maps based on impact parameters constrained by real deposit data. Finally, major improvements will include the further modification of PYFLOW towards an even more user-friendly version with the implementation of a Graphic User Interface.

Acknowledgements Published with permission of the Executive Director of British Geological Survey (NERC). We thank the editor, Andrew Harris, the associate editor, Hannah Dieterich, and the reviewers, Sylvain Charbonnier and Matthew Sweeney, for their great contributions in improving this manuscript. We would like to thank Prof. Pierfrancesco Dellino for the fruitful discussions.

Open Access This article is distributed under the terms of the Creative Commons Attribution 4.0 International License (<http://creativecommons.org/licenses/by/4.0/>), which permits unrestricted use, distribution, and reproduction in any medium, provided you give appropriate credit to the original author(s) and the source, provide a link to the Creative Commons license, and indicate if changes were made.

References

- Bagheri G, Bonadonna C (2016) On the drag of freely falling non-spherical particles. *Powder Technol* 301:526–544. <https://doi.org/10.1016/j.powtec.2016.06.015>
- Baxter PJ, Neri A, Todesco M (1998) Physical modeling and human survival in pyroclastic flows. *Nat Hazards* 17(2):163–176. <https://doi.org/10.1023/A:1008031004183>
- Baxter PJ, Boyle R, Cole P, Neri A, Spence R, Zuccaro G (2005) The impacts of pyroclastic surges on buildings at the eruption of the Soufriere Hills volcano, Montserrat. *Bull Volcanol* 67(4):292–313. <https://doi.org/10.1007/s00445-004-0365-7>
- Beckett FM, Witham CS, Hort MC, Stevenson JA, Bonadonna C, Millington SC (2015) Sensitivity of dispersion model forecasts of

- volcanic ash clouds to the physical characteristics of the particles. *J Geophys Res Atmos* 120(22):11636–11652. <https://doi.org/10.1002/2015JD023609>
- Bevilacqua A, Isaia R, Neri A, Vitale S, Aspinall WP, Bisson M, Flandoli F, Baxter PJ, Bertagnini A, Esposti Ongaro T, Iannuzzi E, Pistolesi M, Rosi M (2015) Quantifying volcanic hazard at Campi Flegrei caldera (Italy) with uncertainty assessment: 1. Vent opening maps. *J Geophys Res Solid Earth* 120(4):2309–2329. <https://doi.org/10.1002/2014JB011775>
- Brand BD, Bendana S, Self S, Pollock N (2016) Topographic controls on pyroclastic density current dynamics: insight from 18 May 1980 deposits at Mount St. Helens, Washington (USA). *J Volcanol Geotherm Res* 321:1–17. <https://doi.org/10.1016/j.jvolgeores.2016.04.018>
- Branney MJ, Kokelaar P (2002) Pyroclastic density currents and the sedimentation of ignimbrites. Geological Society, London, *Memoirs* 27
- Breard ECP, Lube G, Cronin SJ, Valentine GA (2015) Transport and deposition processes of the hydrothermal blast of the 6 August 2012 Te Maari eruption, Mt. Tongariro. *Bull Volcanol* 77(11):100. <https://doi.org/10.1007/s00445-015-0980-5>
- Brown RJ, Kokelaar BP, Branney MJ (2007) Widespread transport of pyroclastic density currents from a large silicic tuff ring: the Glaramara tuff, Scafell caldera, English Lake District, UK. *Sedimentology* 54(5):1163–1189. <https://doi.org/10.1111/j.1365-3091.2007.00877.x>
- Burgisser A, Bergantz GW (2002) Reconciling pyroclastic flow and surge: the multiphase physics of pyroclastic density currents. *Earth Planet Sc Lett* 202(2):405–418. [https://doi.org/10.1016/S0012-821X\(02\)00789-6](https://doi.org/10.1016/S0012-821X(02)00789-6)
- Bursik MI, Woods AW (1996) The dynamics and thermodynamics of large ash flows. *Bull Volcanol* 58(2-3):175–193. <https://doi.org/10.1007/s004450050134>
- Caricchi L, Vona A, Corrado S, Giordano G, Romano C (2014) 79 AD Vesuvius PDC deposits' temperatures inferred from optical analysis on woods charred in-situ in the *Villa dei Papiri* at Herculaneum (Italy). *J Volcanol Geotherm Res* 289:14–25. <https://doi.org/10.1016/j.jvolgeores.2014.10.016>
- Charbonnier SJ, Germa A, Connor CB, Gertisser R, Preece K, Komorowski JC, Lavigne F, Dixon T, Connor L (2013) Evaluation of the impact of the 2010 pyroclastic density currents at Merapi volcano from high-resolution satellite imagery, field investigations and numerical simulations. *J Volcanol Geotherm Res* 261:295–315. <https://doi.org/10.1016/j.jvolgeores.2012.12.021>
- Chien SF (1994) Settling velocity of irregularly shaped particles. *SPE Drill Complet* 9(04):281–288. <https://doi.org/10.2118/26121-PA>
- Chough SK, Sohn YK (1990) Depositional mechanics and sequences of base surges, Songaksan tuff ring, Cheju Island, Korea. *Sedimentology* 37(6):1115–1135. <https://doi.org/10.1111/j.1365-3091.1990.tb01849.x>
- Clift R, Gauvin WH (1971) Motion of entrained particles in gas stream. *Can J Chem Eng* 49(4):439–448. <https://doi.org/10.1002/cjce.5450490403>
- Dellino P, La Volpe L (2000) Structures and grain size distribution in surge deposits as a tool for modelling the dynamics of dilute pyroclastic density currents at La Fossa di Vulcano (Aeolian Islands, Italy). *J Volcanol Geotherm Res* 96(1-2):57–78. [https://doi.org/10.1016/S0377-0273\(99\)00140-7](https://doi.org/10.1016/S0377-0273(99)00140-7)
- Dellino P, Isaia R, Veneruso M (2004) Turbulent boundary layer shear flows as an approximation of base surges at Campi Flegrei (Southern Italy). *J Volcanol Geotherm Res* 133(1-4):211–228. [https://doi.org/10.1016/S0377-0273\(03\)00399-8](https://doi.org/10.1016/S0377-0273(03)00399-8)
- Dellino P, Mele D, Bonasia R, Braia G, La Volpe L, Sulpizio R (2005) The analysis of the influence of pumice shape on its terminal velocity. *Geophys Res Lett* 32(21):L21306. <https://doi.org/10.1029/2005GL023954>
- Dellino P, Zimanowski B, Büttner R, La Volpe L, Sulpizio R (2007) Large-scale experiments on the mechanics of pyroclastic flows: design, engineering, and first results. *J Geophys Res* 112(B4):B04202. <https://doi.org/10.1029/2006JB004313>
- Dellino P, Mele D, Sulpizio R, La Volpe L, Braia G (2008) A method for the calculation of the impact parameters of dilute pyroclastic density currents based on deposit particle characteristics. *J Geophys Res* 113:B07206. <https://doi.org/10.1029/2007B005365>
- Dellino P, Dioguardi F, Zimanowski B, Büttner R, Mele D, La Volpe L, Sulpizio R, Doronzo DM, Sonder I, Bonasia R, Calvari S, Marotta E (2010a) Conduit flow experiments help constraining the regime of explosive eruptions. *J Geophys Res* 115(B4):B04204. <https://doi.org/10.1029/2009JB006781>
- Dellino P, Büttner R, Dioguardi F, Doronzo DM, La Volpe L, Mele D, Sonder I, Sulpizio R, Zimanowski B (2010b) Experimental evidence links volcanic particle characteristics to pyroclastic flow hazard. *Earth Planet Sc Lett* 295(1-2):314–320. <https://doi.org/10.1016/j.epsl.2010.04.022>
- Dellino P, Dioguardi F, Mele D, D'Addabbo M, Zimanowski B, Büttner R, Doronzo DM, Sonder I, Sulpizio R, Dürig T, La Volpe L (2014) Volcanic jets, plumes, and collapsing fountains: evidence from large-scale experiments, with particular emphasis on the entrainment rate. *Bull Volcanol* 76(6):834. <https://doi.org/10.1007/s00445-014-0834-6>
- Dioguardi F, Dellino P (2014). PYFLOW: a computer code for the calculation of the impact parameters of dilute pyroclastic density currents (DPDC) based on field data. *Comput Geosci* 66:200–210. doi: 10.1016/j.cageo.2014.01.013
- Dioguardi F, Dellino P, Mele D (2014) Integration of a new shape-dependent particle–fluid drag coefficient law in the multiphase Eulerian–Lagrangian code MFIX-DEM. *Powder Technol* 260:68–77. <https://doi.org/10.1016/j.powtec.2014.03.071>
- Dioguardi F, Mele D (2015) A new shape dependent drag correlation formula for non-spherical rough particles. Experiments and results. *Powder Technol* 277:222–230. <https://doi.org/10.1016/j.powtec.2015.02.062>
- Dioguardi F, Mele D, Dellino P, Dürig T (2017) The terminal velocity of volcanic particles with shape obtained from 3D X-ray microtomography. *J Volcanol Geotherm Res* 329:41–53. <https://doi.org/10.1016/j.jvolgeores.2016.11.013>
- Doronzo DM, Dellino P (2011) Interaction between pyroclastic density currents and buildings: numerical simulation and first experiments. *Earth Planet Sc Lett* 310(3-4):286–292. <https://doi.org/10.1016/j.epsl.2011.08.017>
- Doronzo DM (2012) Two new end members of pyroclastic density currents: forced convection-dominated and inertia-dominated. *J Volcanol Geotherm Res* 219-220:87–91. <https://doi.org/10.1016/j.jvolgeores.2012.01.010>
- Dufek J (2016) The fluid mechanics of pyroclastic density currents. *Annu Rev Fluid Mech* 48(1):459–485. <https://doi.org/10.1146/annurev-fluid-122414-034252>
- Engwell S, de' Michieli Vitturi M, Esposti Ongaro T, Neri A (2016) Insights into the formation and dynamics of coignimbrite plumes from one-dimensional models. *J Geophys Res Solid Earth* 121(6):4211–4231. <https://doi.org/10.1002/2016JB012793>
- Esposti Ongaro T, Cavazzoni C, Erbacci G, Neri A, Salvetti MV (2007) A parallel multiphase flow code for the 3D simulation of explosive volcanic eruptions. *Parallel Comput* 33(7-8):541–560. <https://doi.org/10.1016/j.parco.2007.04.003>
- Furbish DJ (1997) Fluid physics in geology. Oxford University Press, New York
- Ganser G (1993) A rational approach to drag prediction of spherical and nonspherical particles. *Powder Technol* 77(2):143–152. [https://doi.org/10.1016/0032-5910\(93\)80051-B](https://doi.org/10.1016/0032-5910(93)80051-B)
- Gurioli L, Cioni R, Sbrana A, Zanella E (2002) Transport and deposition of pyroclastic density currents over an inhabited area: the deposits of

- the AD 79 eruption of Vesuvius at Herculaneum, Italy. *Sedimentology* 49(5):929–953. <https://doi.org/10.1046/j.1365-3091.2002.00483.x>
- Haider A, Levenspiel O (1989) Drag coefficient and terminal velocity of spherical and nonspherical particles. *Powder Technol* 58(1):63–70. [https://doi.org/10.1016/0032-5910\(89\)80008-7](https://doi.org/10.1016/0032-5910(89)80008-7)
- Hölzer A, Sommerfeld M (2008) New simple correlation formula for the drag coefficient of non spherical particles. *Powder Technol* 184(3):361–365. <https://doi.org/10.1016/j.powtec.2007.08.021>
- Horwell CJ, Baxter P (2006) The respiratory health hazards of volcanic ash: a review for volcanic risk mitigation. *Bull Volcanol* 69(1):1–24. <https://doi.org/10.1007/s00445-006-0052-y>
- Houghton BF, Wilson CJN (1989) A vesicularity index for pyroclastic deposits. *Bull Volcanol* 51(6):451–462. <https://doi.org/10.1007/BF01078811>
- Inman DL (1952) Measures of describing the size distribution of sediments. *J Sediment Petrol* 22:125–145
- Iverson RM, Vallance JM (2001) New views of granular mass flows. *Geology* 29(2):115–118. [https://doi.org/10.1130/0091-7613\(2001\)029<0115:NVGOMF>2.0.CO;2](https://doi.org/10.1130/0091-7613(2001)029<0115:NVGOMF>2.0.CO;2)
- Jenkins S, Komorowski JC, Baxter PJ, Spence R, Picquout A, Lavigne F, Surono (2013) The Merapi 2010 eruption: an interdisciplinary assessment methodology for studying pyroclastic density currents. *J Volcanol Geotherm Res* 261:316–329
- L'Abbate A (2007) Calcolo dei parametri fisici di “correnti piroclastiche di densità” naturali e prodotte in esperimenti. University of Bari, Bari, Italy, Msc Dissertation.
- Leeder ME, Gray TE, Alexander J (2005) Sediment suspension dynamics and a new criterion for the maintenance of turbulent suspensions. *Sedimentology* 52(4):683–691. <https://doi.org/10.1111/j.1365-3091.2005.00720.x>
- Lube G, Breard ECP, Cronin SJ, Jones J (2015) Synthesizing large-scale pyroclastic flows: experimental design, scaling, and first results from PELE. *J Geophys Res Solid Earth* 120(3):1487–1502. <https://doi.org/10.1002/2014JB011666>
- Manzaro C (2005) Ricostruzione delle dinamiche eruttive del vulcano Astroni (Campi Flegrei). University of Bari, Bari, Italy, MSc Dissertation
- Mele D, Dioguardi F, Dellino P, Isaia R, Sulpizio R, Braia G (2015) Hazard of pyroclastic density currents at the Campi Flegrei Caldera (Southern Italy) as deduced from the combined use of facies architecture, physical modeling and statistics of the impact parameters. *J Volcanol Geotherm Res* 299:35–53. <https://doi.org/10.1016/j.jvolgeores.2015.04.002>
- Middleton GV, Southard JB (1984) *Mechanics of sediment movement*, 2nd edn. Society of Economic Paleontologists and Mineralogists, Tulsa, OK. <https://doi.org/10.2110/scn.84.03>
- Miller MC, McCave IN, Komar PD (1977) Threshold of sediment motion under unidirectional currents. *Sedimentology* 24(4):507–527. <https://doi.org/10.1111/j.1365-3091.1977.tb00136.x>
- Neri A, Esposti Ongaro T, Macedonio G, Gidaspow D (2003) Multiparticle simulation of collapsing volcanic columns and pyroclastic flow. *J Geophys Res* 108(B4):2202. <https://doi.org/10.1029/2001JB000508>
- Neri A, Esposti Ongaro T, Monconi G, de' Michieli Vitturi M, Cavazzoni C, Erbacci G, Baxter PJ (2007) 4D simulation of explosive eruption dynamics at Vesuvius. *Geophys Res Lett* 34(4):L04309. <https://doi.org/10.1029/2006GL028597>
- Neri A, Esposti Ongaro T, Voight B, Widiwijayanti C (2015a) Pyroclastic density current hazards and risk. In: Papale P, Shroder JF (eds) *Volcanic hazards, risks and disasters*. Elsevier, Amsterdam, pp 109–140. <https://doi.org/10.1016/B978-0-12-396453-3.00005-8>
- Neri A, Bevilacqua A, Esposti Ongaro T, Isaia R, Aspinall WP, Bisson M, Flandoli F, Baxter PJ, Bertagnini A, Iannuzzi E, Orsucci S, Pistolesi M, Rosi M, Vitale S (2015b) Quantifying volcanic hazard at Campi Flegrei caldera (Italy) with uncertainty assessment: 2. Pyroclastic density current invasion maps. *J Geophys Res Solid Earth* 120(4):2330–2349. <https://doi.org/10.1002/2014JB011776>
- Nield SE, Woods AW (2003) Effects of flow density on the dynamics of dilute pyroclastic density currents. *J Volcanol Geotherm Res* 132:269–281
- Pope SB (2000) *Turbulent flows*. Cambridge University Press. <https://doi.org/10.1017/CBO9780511840531>
- Roche O (2012) Depositional processes and gas pore pressure in pyroclastic flows: an experimental perspective. *Bull Volcanol* 74(8):1807–1820. <https://doi.org/10.1007/s00445-012-0639-4>
- Rouse H (1939) An analysis of sediment transportation in the light of fluid turbulence. Soil Conservation Services Report No. SCS-TP-25, USDA, Washington, D.C.
- Schlichting H, Gersten K (2000) *Boundary-layer theory*. Springer, Berlin. <https://doi.org/10.1007/978-3-642-85829-1>
- Stow DAV, Bowen AJ (1980) A physical model for the transport and sorting of fine-grained sediment by turbidity currents. *Sedimentology* 27(1):31–46. <https://doi.org/10.1111/j.1365-3091.1980.tb01156.x>
- Sulpizio R, Mele D, Dellino P, La Volpe L (2005) A complex, Subplinian-type eruption from low-viscosity, tephri-phonolitic magma: the Pollena eruption of Somma-Vesuvius (Italy). *Bull Volcanol* 67(8):743–767. <https://doi.org/10.1007/s00445-005-0414-x>
- Sulpizio R, Mele D, Dellino P, La Volpe L (2007) Deposits and physical properties of pyroclastic density currents during complex Subplinian eruptions: the AD 472 (Pollena) eruption of Somma-Vesuvius, Italy. *Sedimentology* 54(3):607–635. <https://doi.org/10.1111/j.13653091.2006.00852.x>
- Sulpizio R, Dellino P (2008) Sedimentology, depositional mechanisms and pulsating behavior of pyroclastic density currents. In: Marti J, Gottsman J (eds) *Calderas volcanism: analysis, modelling and response*. Vol. 10, developments in volcanology. Elsevier, Amsterdam, pp 57–96. [https://doi.org/10.1016/S1871-644X\(07\)00002-2](https://doi.org/10.1016/S1871-644X(07)00002-2)
- Sulpizio R, Dellino P, Doronzo DM, Sarocchi D (2014) Pyroclastic density currents: state of the art and perspectives. *J Volcanol Geotherm Res* 283:36–65. <https://doi.org/10.1016/j.jvolgeores.2014.06.014>
- Sulpizio R, Castioni D, Rodriguez-Sedano LA, Sarocchi D, Lucchi F (2016) The influence of slope-angle ratio on the dynamics of granular flows: insights from laboratory experiments. *Bull Volcanol* 78(11):77. <https://doi.org/10.1007/s00445-016-1069-5>
- Swamee PK, Ojha CP (1991) Drag coefficient and fall velocity of non-spherical particles. *J Hydraul Eng* 117(5):660–669. [https://doi.org/10.1061/\(ASCE\)0733-9429\(1991\)117:5\(660\)](https://doi.org/10.1061/(ASCE)0733-9429(1991)117:5(660))
- Tran-Cong S, Gay M, Michaelides EE (2004) Drag coefficients of irregularly shaped particles. *Powder Technol* 139(1):21–32. <https://doi.org/10.1016/j.powtec.2003.10.002>
- Valentine GA (1987) Stratified flow in pyroclastic surges. *Bull Volcanol* 49(4):616–630. <https://doi.org/10.1007/BF01079967>
- Wilson CJN (1980) The role of fluidization in the emplacement of pyroclastic flows: an experimental approach. *J Volcanol Geotherm Res* 8(2-4):231–249. [https://doi.org/10.1016/0377-0273\(80\)90106-7](https://doi.org/10.1016/0377-0273(80)90106-7)
- Woods AW, Bursik MI (1994) A laboratory study of ash flows. *J Geophys Res* 99(B3):4375–4394. <https://doi.org/10.1029/93JB02224>